Growth of defect free GaP nanowires

Elena Husanu[1], Daniele Ercolani[1], Mauro Gemmi[2], and Lucia Sorba[1]

1. NEST Scuola Normale Superiore and Istituto di Nanoscienze-CNR, P.zza S. Silvestro 12,I-56127 PISA, Italy

2. Center for Nanotechnology Innovation @ NEST, Istituto Italiano di Tecnologia, P.zza S. Silvestro 12, I-56127 Pisa,Italy

Abstract

The crystal structure of GaP nanowires grown by Au-assisted chemical beam epitaxy was investigated as a function of group V flux and growth temperature. By increasing the tertiarybutyl phosphine flux we obtained nanowires with stacking defect-free wurtzite crystal structure. Variation of growth temperature had also a profound impact on the crystal structure. Lowering the growth temperature from 600 to 560 °C and keeping constant both triethylgallium and tertiarybutyl phosphine precursor fluxes, the crystal structure of GaP NWs was drastically improved from a highly defective intergrowth of zinc-blende and wurtzite to a wurtzite crystal structure free of stacking defects. These results are compared to current literature on GaP NW growth, and we suggest that the low V/III ratio is the key ingredient for the high crystal quality of our GaP nanowires.

1. Introduction

III-V semiconductor nanowires (NWs) are one dimensional building blocks with potential applications in future devices and systems. The epitaxial growth of these nanostructures allows unprecedented flexibility in the combination of materials thanks to the strain release on the surface [1]. Such heterostructures are of potential interest because they allow integration of materials that are suitable for optoelectronic applications [2,3] solar cells [4], lasers [5] and light emitting diodes [6]. Recent studies have highlighted the influence of the crystal structure on the electronic and optical properties [7,8,9] of III-V NWs. Indeed, the development of NW-based devices depends on the ability to tightly control properties such as morphology, crystal structure, and composition. On the other hand, despite the different growth methods such as molecular beam epitaxy (MBE), chemical beam epitaxy (CBE), metalorganic vapor phase epitaxy (MOVPE), etc., and the variety of material systems explored [10,11,12,16] the NW crystal quality is often poor and difficult to control, and depends critically on growth temperature, NW diameter, growth rate, and III-V ratio. Commonly reported defects in NWs are twin defects, stacking faults, wurtzite-zincblende polytypism. All these are attenuating or disrupting the optical and electronic properties of the NWs [13]. A stacking fault in a wurtzite (WZ) NW growing along the *c*-axis can be described by the sequence …AB**ABC**BCB…, where the highlighted ABC sequence corresponds to the typical zincblende (ZB) stacking. In a ZB NW growing along the [111] direction the most common crystal defect is the so-called twin plane, described by the sequence …ABC**ABA**CB..., where we have highlighted a short WZ sequence (ABA). Thus, the presence and density of stacking defects in NWs is closely related to how stable the WZ or ZB phase is in the kinetic and thermodynamic conditions of growth. Although most bulk III-V materials present a ZB crystal structure, in the case of NWs both WZ and ZB crystal structures are easily found. The stability of WZ and ZB phases in III-V semiconductors was

found to be strongly dependent on the ionicity of chemical bonds, high ionicity favoring WZ and low ionicity ZB crystal structure [14]. It is generally accepted that among III-V binaries GaN has the highest ionicity and can be synthesized in WZ arrangement even in bulk crystals. At the opposite extreme, antimonides have the lowest ionicity and are forming a ZB crystal phase even in thin NWs [1,15]. Arsenides and phosphides have intermediate ionicity values, and nanowires based on these materials are presenting mixed WZ-ZB crystal structures [16].

A vast theoretical and experimental literature has investigated the formation mechanisms and the strategies for reduction of stacking defects in NWs, with particular focus on InAs and GaAs [17,18]. Galika and coworkers studied by *ab initio* methods the stability of WZ and ZB phase in NWs with thin diameters (up to 10 nm) concluding that NWs with diameters up to 5 nm adopt a WZ structure [17]; similar results have been obtained by an empirical potential approach [18] setting the diameter threshold in the 12-32 nm range, depending on the NW constituents. Although clearly predicting the qualitative trend (WZ for thin NWs and ZB for thick ones) these studies underestimate the critical diameters for the transition, since it is not at all uncommon to find WZ NWs in the 100 nm diameter range. Glas and coworkers developed a model considering the catalyst particle alloy supersaturation (intended as the difference in the chemical potential between the supply phase and the growing phase): at low (high) supersaturation, i.e. with low (high) Ga content in the AuGa particle, ZB (WZ) structure is favored [19]. Dubrovskii and coworkers integrated both diameter and supersaturation dependence of the crystal structure in a single model [20].

GaP has been comparatively less studied, and so far very few defect-free GaP NWs have been reported in literature [9]. Predominantly WZ GaP NWs with stacking faults have been grown by MBE [21,22], obtaining ZB only at low supersaturation and large NW diameters. As for MOVPE, Verheijein and coworkers have shown that GaAs-GaP NWs have

defected ZB crystal structure that is unaffected by growth temperature or precursor flux variation in the studied ranges [23]. Others have instead shown that varying the alloy supersaturation during GaP NW growth they could obtain ZB NWs with twins or WZ NWs with stacking faults [24], and GaP NW crystal phase have been switched from WZ to ZB by increasing the group V flow by 50-150 times [25]. More recently, by combining high supersaturation and high growth temperature with *in situ* HCl etching to suppress radial growth, high crystalline quality WZ GaP and core-shell GaP-AlGaP have been grown by MOVPE [9].

In what follows we will discuss the CBE growth of GaAs-GaP nanowire heterostructures, focusing our attention on the crystal phase and stacking defect density of the GaP segment. The nanowires were grown using Au as catalyst varying the growth temperature and phosphor precursor flux. Crystal phase determination and defect density analysis have been performed with transmission electron microscopy imaging coupled with selected area electron diffraction (SAED). We will show that it is possible to synthesize long WZ GaP NWs that are free of stacking defects, and this is due to the low V/III ratio at which our CBE growth takes place.

2. Methods

All GaAs/GaP NW growths were performed by Au-assisted CBE in a Riber Compact 21 system. The system employs pressure control in the metalorganic (MO) lines to determine precursor fluxes during the sample growth. The precursors involved in the NW growth are triethylgallium (TEGa), tertiarybuthyl arsine (TBAs) and tertiarybuthyl phosphine (TBP). Due to their high decomposition temperature, TBAs and TBP were pre-cracked in the injector at 1000 °C.

A nominally 0.5 nm thick Au film was first deposited on (111)B GaAs wafers by thermal evaporation in a separate evaporator chamber and then transferred to the CBE growth

chamber. Before initiating the growth, the samples were heated at 560 °C under TBAs flow for 20 min in order to dewet the Au film into nanoparticles and to remove the surface oxide from the GaAs substrate. The growth temperature of the GaAs stem (560 °C) was fixed for all samples. The MO line pressures were 0.7 and 1 Torr for TEGa and TBAs, respectively. The GaAs stem was grown for 60 min leading to ~ 1 um long GaAs segment with an average diameter of 50 nm. During the last 10 min of GaAs growth the temperature was linearly ramped to reach the desired GaP growth temperature. The growth was continued for another 20 min by keeping TEGa line pressure at 0.7 Torr and switching off abruptly TBAs flux and opening TBP flux. For the GaP segment the TBP line pressure was varied from sample to sample between 1 and 6 Torr. The GaP segments were grown in a large temperature interval from 560 °C to 660 °C. The growth was ended by switching off the TEGa flux and cooling the sample under TBP flux.

TEM observations were carried with a Zeiss Libra 120 TEM operating at an accelerating voltage of 120 kV. The samples for TEM analysis have been mechanically transferred onto copper TEM grids coated with a formvar carbon film by gently rubbing the grids on the as-grown substrate. Bright Field TEM (BFTEM) coupled with SAED has been used for crystal structure determination and defect analysis. Scanning TEM (STEM) was employed for accurate GaP segment length determination.

3. Results and discussion

A crystal structure characterization of GaP NWs requires to identify the ZB and WZ polytypes, to detect the presence of stacking defects and twinning and to determine the specific location of these in the NW body. The crystal structure type has been determined by SAED collected in $[2\text{-}1\text{-}10]_{WZ}$ (parallel to $[110]_{ZB}$) zone axis. In this orientation the patterns of ZB and WZ crystal structures do not superimpose and can be easily distinguished. For the same reason a BFTEM image taken in the same orientation allows to visualize the presence

of stacking faults and polytype changes as sharp changes in the image contrast [26]. To ensure consistence and reproducibility of our results, at least 10 NWs were analyzed for each sample.

TEM observations indicate that, depending on the growth conditions, the GaP segments goes from a highly defective structure formed by a dense intergrowth of WZ and ZB thin sectors to a stacking defect free WZ structure.

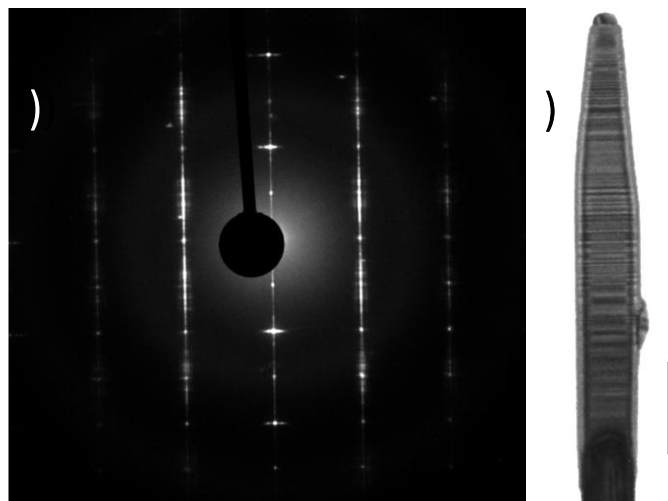

Figure 1. (a) SAED pattern acquired from an area of 300 nm in diameter in the center of the GaP section of the NW shown in (b). The pattern cannot be indexed unambiguously as $[2-1-10]_{WZ}$ or $[110]_{ZB}$ zone axis due to stacking disorder which causes streaking along $(0001)_{ZB}$ reciprocal direction. (b) BFTEM overview image of a GaP segment grown at 600°C with a TBP line pressure of 1 Torr. Scale bar 100 nm.

Figure 1(a) shows a SAED pattern of a GaP NW segment grown at 600 °C with TEGa and TBP line pressures of 0.7 and 1 Torr, respectively, while figure 1(b) shows a BF image of the same NW. The SAED pattern cannot be indexed unambiguously because it contains signatures of both a $[2-1-10]_{WZ}$ of a WZ crystal and $[110]_{ZB}$ of a ZB crystal zone axis. The streaking and multiple spots are due to a disordered sequence of stacking faults and thin WZ and twinned ZB segments. This is confirmed by the corresponding bright field image (figure 1(b)) that shows an alternate arrangement of bright and dark contrast stripes (normal to the NW growth axis) over the entire length of the GaP segment. A small section of the GaAs

stem is visible at the bottom of the NW as a segment with distinctly darker contrast. The GaAs stems of all samples presented here have WZ structure with densely packed stacking faults. This highly defective structure is consistent with the current literature [21-25], where reports of defect-free WZ GaP NWs are not frequent [9].

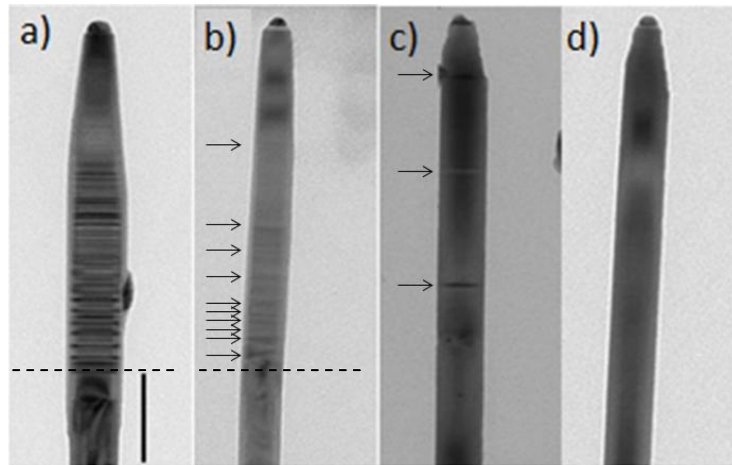

Figure 2. Bright field TEM images corresponding to the GaP segment grown at 600 ^{0}C: (a) P_{TBP} =1 Torr, (b) P_{TBP} =2 Torr, (c) P_{TBP} =3 Torr, and (d) P_{TBP} =4 Torr. Scale bar –common to all 4 micrographs– corresponds to 100 nm. The arrows in (b) an (c) indicate the defects that are visible in the GaP part. The dashed line indicates the interface between the GaAs and the GaP segments.

By keeping the GaP growth temperature constant at 600 °C and varying the TBP line pressure (P_{TBP}) from 1 to 4 Torr in steps of 1 Torr, it was possible to clearly observe the effect of an increasing group V to group III (V/III) flux ratio on the structural characteristics of GaP NWs. The BFTEM images of representative NWs of the four samples are shown in figure 2, in order of increasing TBP line pressure. In figure 2(a-b) a dashed line marks the GaAs/GaP interface. The GaAs stem is at the bottom part and systematically shows a modulated changing contrast arising from strain modulation due to the growth of a thin GaP shell around the GaAs core. GaP segments of the samples shown in figure 2(c-d) are much longer (as discussed later and shown in figure 5) and therefore GaAs/GaP interface lies outside the micrograph. The black arrows in Fig 2(b-c) mark the stacking defects in the GaP segment. It is clear that at higher TBP line pressure the defect density is reduced to a negligible amount.

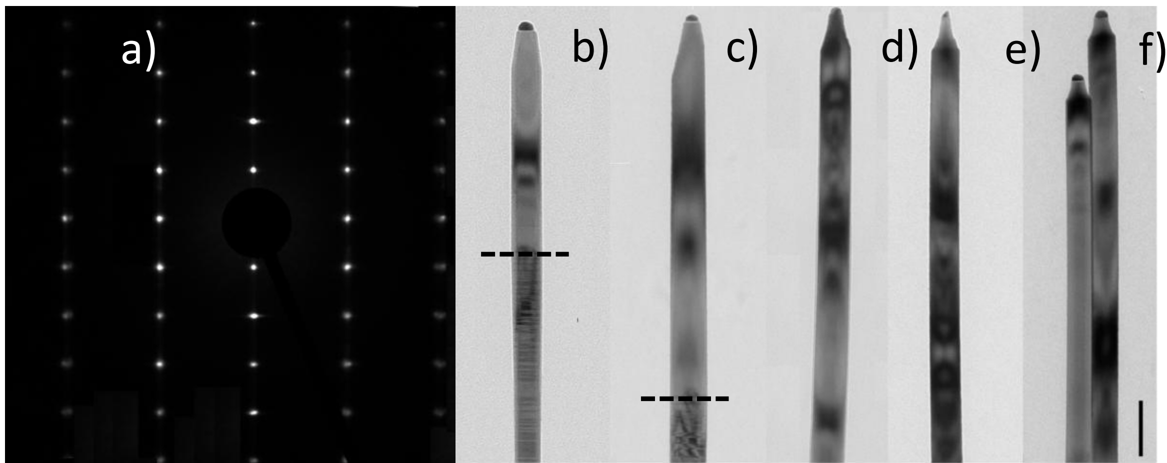

Figure 3. Bright-field TEM images and SAED corresponding to GaP segment grown at 560 ^{0}C: (a) SAED pattern of a GaP segment grown with TBP pressure 1 Torr;(b)-(f) BF images of GaP segments grown with different TBP fluxes: (b) P_{TBP} =1 Torr, (c) P_{TBP} =2 Torr, (d) P_{TBP} =3 Torr, (e) P_{TBP}=4 Torr, and (f) P_{TBP}= 6 Torr. The dashed lines indicate the interface between GaAs and GaP segments. Scale bar, common to all micrographs, corresponds to 100 nm.

At a lower growth temperature (560 °C) the GaP segment appears to be defect free in the whole TBP line pressure range from 1 to 6 Torr. The BFTEM images of NWs grown at this temperature are displayed in figure 3(b-f) together with one SAED pattern (figure 3(a)) collected on the NW of figure 3b, grown with TEGa and TBP line pressures of 0.7 and 1 Torr, respectively. The pattern, which is representative also for the other samples, can be indexed as $[2\text{-}1\text{-}10]_{WZ}$ zone axis of a WZ crystal structure, and there is no signature of ZB diffraction spots nor the typical streaking parallel to the (0001) reciprocal direction, which would indicate the presence of stacking defects. In figure 3(b-c) we can also clearly distinguish the GaAs/GaP interface: the bottom part with periodical stacking faults corresponds to the GaAs stem, while the clean upper part belongs to GaP. The large shadow fringes in the GaP segments are bend contours, i.e. contrast due to the bending of the flexible wire. The sharp neck under the catalyst is likely to be the consequence of the cooling of the NWs under TBP flow: NW growth continues and consumes the Ga supply in the AuGa droplet, reducing its size [27].

An increase in GaP growth temperature from 620 to 660 °C, does not improve the structural characteristics of the crystal but the morphology strongly changes. In particular the density of straight nanowires is greatly diminished, and at 660 °C most NWs were growing with GaP segment kinked (see figure 4(b)).

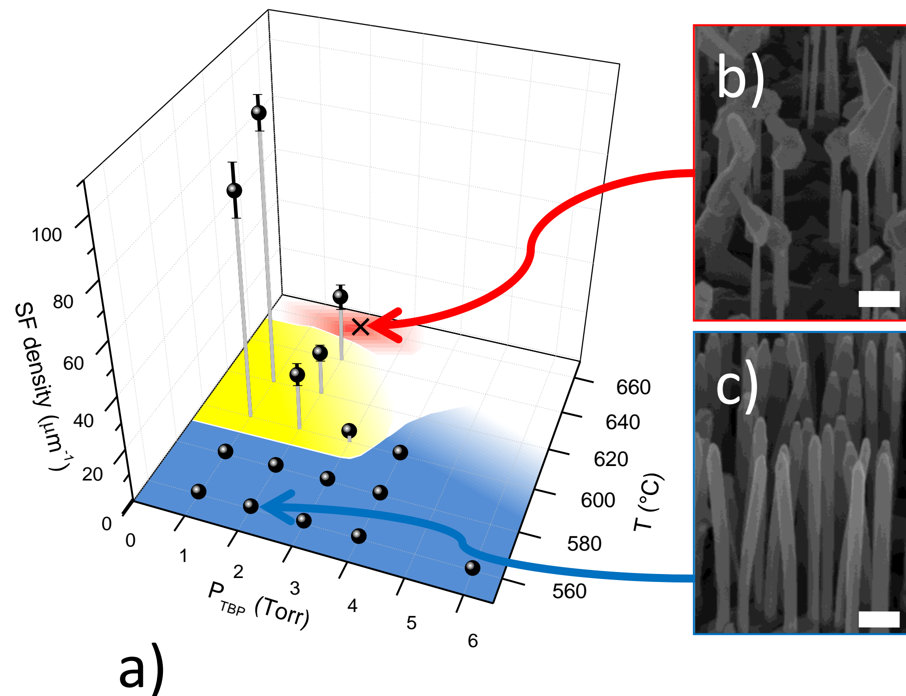

Figure 4. Growth parameter dependence of the crystal structure of GaP NWs. (a) plot of the density of stacking faults in the WZ crystal structures of all GaP NWs analyzed in the present work, as a function of TBP line pressure and growth temperature. The stacking faults have been counted on BFTEM images of at least 10 NWs per sample. Error bars represent the uncertainty derived as a statistical counting error on stacking fault number count. The different colors in the parameter plane represent WZ GaP NWs with no stacking faults (blue), with stacking faults (yellow), and with other morphological issues (red). (b) and (c) are 45° tilted scanning electron micrographs of the samples grown with P_{TBP}=2 Torr, and T=660 and 560 °C, respectively. Scale bars are 200 nm.

Figure 4 summarizes how growth temperature and TBP flux are influencing the crystal structure of our CBE grown GaP NWs. No pure ZB phase is observed in the whole growth parameter space. This is very interesting since most research groups observe ZB crystal structure in GaP NWs regardless of the growth method and for most of the growth conditions: supercritical fluid-liquid-solid synthesis [28], MOVPE [23,24,29,16,30], or gas source MBE (GSMBE) [22]. Notable exceptions, in which a WZ structure has been reported,

are GaP cores of GaP/GaAs core/multishell NWs grown by MOVPE at high temperature and low V/III ratio [31], short GaP segments of GaAs/GaP [22] multiple heterostructured NWs, GaP/GaAsP [21,32] NW heterostructures grown by GSMBE at relatively high temperatures, and WZ/ZB switching by increasing the PH_3 flow by two orders of magnitude in MOVPE [25], and almost defect-free GaP and core/shell GaP/AlGaP grown by MOVPE at high V/III ratio and high temperature. In our experiments, we observe GaP NWs with defect free WZ crystal structure at the lower growth temperatures (560-580 °C) regardless of the TBP line pressure employed, and this for the whole length of the NW (well in excess of 1 μm, see figure 5). When moving to higher growth temperatures (600°C), stacking faults appear, but their density decreases with increasing TBP line pressure, and we obtain stacking fault-free WZ GaP NWs again for the highest TBP flux. At even higher temperatures the trend is similar, but other morphological changes appear (kinks and other macroscopic defects, see figure 4(b) compared to figure 4(c), representative of the samples grown at lower temperature), making stacking fault density determination difficult if not impossible. The colored areas in figure 4(a) help to map the various regions of the parameter space: blue for stacking fault free GaP, yellow for defected GaP, and red for kinked wires.

Our results appear to be in contrast with most of the WZ/ZB literature up to date. A widely shared opinion is that that for III-V NWs in general (and also for GaP), a low group III content in the Au-III droplet (i.e. low supersaturation, low chemical potential, high V/III ratio) is favoring ZB over WZ. This is observed either as a reduction of twins in ZB, or a increase in stacking faults in WZ or even as a switching from WZ to ZB as the predominant phase [19,31,30,24,25]. However, a number of works indicate that at least in GaP and GaAs, the ZB phase can be favored both at high and low supersaturation, with WZ occupying the intermediate range [21,22,27,322]. We argue that in our CBE system and in the growth conditions described in the present work we are obtaining WZ GaP at low V/III ratio, as

opposed to most previous works. Being in the low V/III ratio limit of the WZ range, a decrease of V/III ratio moves the balance towards the formation of ZB phase, with a consequent increase in stacking fault density in our WZ GaP NWs (i.e. short ZB segments, as explained in the introduction). This argument is supported by a number of considerations:

1. Our GaP NW growth rate is P-limited, and thus the catalyst particles must be in a Ga-rich condition. This is made evident by the linear increase of the GaP NW length as a function of the TBP line pressure displayed in Fig. 5, and showing a saturation at P_{TBP} =6 Torr (by keeping all other growth parameters constant: TEGa line pressure, growth time, growth temperature, and GaAs stem).

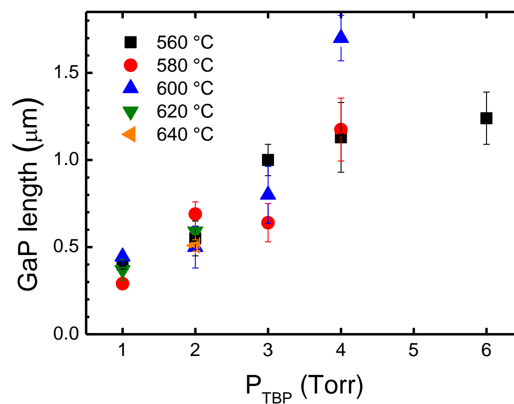

Figure 5. Total GaP segment length as a function of TBP line pressure. Growth temperatures are indicated by the different symbols. All other growth parameters (including growth time, 20 min) are kept constant. Length have been inferred from STEM micrographs, and they are the result of an average over at least 10 NWs per sample. Error bars are the standard deviations.

2. In our GaP NW samples, a stacking defect-free WZ phase is present for lower temperatures, indicating that higher temperatures tend to favor the ZB crystal structure.

3. At the highest growth temperatures, where GaP kinked NWs are predominant, we observe a clear increase in AuGa particle size, suggesting an increased supersaturation related to a stacking fault density increase in WZ.

The reasons why we are working in this rather unexplored V/III ratio regime can be tracked to various fundamental differences in our growth protocol with respect to what is

generally employed for GaP NW growth. Firstly, with CBE we are in a completely different regime with respect to the more common MOVPE: growth pressure is in the high vacuum regime (~10^{-5}-10^{-6} mbar range) allowing for ballistic molecular beams of precursors instead of a diffusive flow. Secondly, the V group precursor we use (1000 °C-cracked TBP) supplies mainly P_4, P_2, and smaller amounts of PH_3 [33] to the growth front, as opposed to PH_3-only as used by most other growth techniques. Thirdly, our Ga precursor (TEGa) undergoes a fairly clean decomposition pathway, leaving byproducts that are unlikely to incorporate in the growing NW, as opposed to the trimetilgallium (TMGa) used in most MOVPE experiments. All these factors together substantially change the conditions during NW growth and are likely to push our system in a thermodynamic scenario which may be hard-to-reach with more common growth techniques. Such scenario may be either the consequence of a high supersaturation of the III-Au alloy particle or of a change in liquid/vapor interface energy.

4. Conclusions

We have studied the CBE growth of GaP NWs and their crystal structure and morphology was investigated in detail by means of bright field TEM and SAED. We have shown that by a careful choice of the growth parameters (precursor fluxes and growth temperature) stacking fault-free WZ GaP NWs can be grown. Interestingly, in contrast to most literature, an increase in supersaturation of the AuGa particles or an increase in growth temperature leads to the appearance of stacking faults and small ZB insertions. We argue that the reason for this behavior is to be found in the unusually low V/III ratio used in our growth which, added to a combination of specific precursors and growth technique leads to either a high alloy particle supersaturation or a significant change in liquid/vapor interface energy.

Since for NW-based devices the high structural quality of the NWs is a fundamental issue, our findings provide useful information to realize long and uniform defect-free WZ GaP NWs, fundamental building blocks for highly efficient nanodevices.

5. Acknowledgments

The work was partly supported by the Marie Curie Initial Training Action (ITN) Q-NET 264034 and by MIUR under PRIN 2009 prot. 2009HS2F7N_003.

[1] Ercolani D, Rossi F,.Li A, Roddaro S, Grillo V, Salviati G, Beltram F, Sorba L, 2009, *Nanotechnology*, **20**, 505605

[2] Li Y, Qian F, Xiang J, Lieber C M, 2006, *Materials Today* **9** (10), 29

[3] Chuang L C, Moewe M, Chase C, Kobayashi N P, Chang-Hasnain C, 2007, *Appl. Phys. Lett.* **90**, 043115

[4] Muskens O L, Gómez Rivas J, Algra R E, Bakkers E P A M, Lagendijk, A, 2008, *Nano Lett.* **8**, 2638

[5] Duan X, Huang Y, Agarwal R, Lieber C M, 2003, *Nature*, **421**, 241

[6] Fukui T, Yoshimura M, Nakai E, Tomioka K, 2012, *Ambio*, **41** (2 supplement), 119

[7] Panda J K, Roy A, Gemmi M, Husanu E, Li A, Ercolani D, Sorba L, 2013, *Appl. Phys. Lett.*, **103**, 023108

[8] Funk S, Li A, Ercolani D, Gemmi M, Sorba L, Zardo I, 2013, *ACS Nano*, **7**, 1400

[9] Assali S et al., 2013, Direct Band Gap Wurtzite Gallium Phosphide Nanowires, *Nano Lett.*, **13**, 1559

[10] Pitanti A, Ercolani D, Sorba L, Roddaro S, Beltram F, Nasi L, Salviati G, Tredicucci A, *Phys. Rev. X,* **1**, 011006

[11] Fakhr A, Haddara Y M, LaPierre R R, 2010, *Nanotechnology*, **21**, 165601

[12] Ercolani D, Gemmi M, Nasi L, Rossi F, Pea M, Li A, Salviati G, Beltram F, Sorba L, 2012, *Nanotechnology*, **23**, 115606

[13] Woo R L, Xiao R, Kobayashi Y, Gao L, Goel N, Hudait M K, Mallouk T E, Hicks R F, 2008, *Nano Lett.*, **8**, 4664

[14] Christensen N E, Satpathy S, Pawlowzka Z, 1987, *Phys Rev B*, **36**, 1032-1050

[15] Caroff P, Messing M E, Borg M, Dick K A , Deppert K, Wernersson L E, 2009, *Nanotechnology*, **20**, 495606

[16] Dick K A, Caroff P, Bolinsson J, Messing M E, Johansson J, Deppert K, Wallenberg L R, Samuelson L, 2010, *Semicond. Sci. Technol.*, **25**, 024009

[17] Galicka M, Bukała M, Buczko R, Kacman P, 2008, *J. Phys.: Condens. Matter.*, **20**, 454226

[18] Akiyama T, Sano K, Nakamura K, Ito T, 2006, *Jpn. J. Appl. Phys.*, **45**, L275

[19] Glas F, Harmand J-C, Patriarche G, 2007, *Phys. Rev. Lett.*, **99**, 146101

[20] Dubrovskii V G, Sibirev N V, Harmand J C, Glas F, 2008, *Phys. Rev. B*, **78**, 235301

[21] Mohseni P K, Maunders C, Botton G A, LaPierre R R, 2007, *Nanotechnology*, **18**, 445304

[22] Boulanger J P and LaPierre R R, 2011, *J. Cryst. Growth*, **332**, 21-26

[23] Verheijen M A, Immink G, de Smet T, Borgström M T, Bakkers E P A M, 2006, *J. Am. Chem. Soc.*, **128**, 1353

[24] Johansson J, Karlsson L S, Dick K A, Bolinsson J, Wacaser B A, Deppert K, Samuelson L, 2009, *Cryst. Growth. Des*., **9**, 766

[25] Lehmann S, Wallentin J, Jacobsson D, Deppert K, Dick K A, 2013, *Nano Lett.*, **13**, 4099

[26] Panda K J, Roy A, Singha A, Gemmi M, Ercolani D, Pellegrini V, Sorba L, 2012, *Appl. Phys. Lett.,* **100**, 143101

[27] Persson A I, Larsson M W, Stenström S, Ohlsson B J, Samuelson L, Wallenberg L R, 2004, *Nat. Mater.*, **3**, 677

[28] Davidson F M, Wiacek R, Korgel B A, 2005, *Chem. Mater.*, **17**, 230

[29] Algra R E, Verheijen M A, Feiner L-F, Immink G G W, van Enckevort W J P, Vlieg E, Bakkers E P A M, 2010, *Nano Lett.*, **10**, 2349

[30] Algra R E, Verheijen M A, Feiner L-F, Immink G G W, van Enckevort W J P, Vlieg E, Bakkers E P A M, 2011, *Nano Lett.*, **11**, 1259

[31] Verheijen M A, Algra R E, Borgström M T, Immink G, Sourty E, van Enckevort W J P, Vlieg E, Bakkers E P A M, 2007, *Nano Lett.*, **7**, 3051

[32] Mohseni P K and LaPierre R R, 2009, *Nanotechnology*, **20**, 025610

[33] D. Ritter, H. Heinecke, 1997, *J. Cryst. Growth*, **170**, 149